International Journal of Progressive Sciences and Technologies (IJPSAT)
ISSN: 2509-0119.

https://ijpsat.org/
Vol. 53 No. 1 October 2025, pp. 378-395

Electrical Performance Of A Standalone Dual-Fluid CPVT Solar Power Plant With MPPT, Buck-Boost Converter, And Battery Storage

PASERA Joanès Keneddy[1], HARITHI BEN Daoud Ben Attoumane[2], DONA Victorien Bruno[3]

[1]Ph.D. Scholar, Laboratory of Applied Physics and Renewable Energies (LPADER), Ecole Doctorale Génie du Vivant et Modélisation (EDGVM), University of Mahajanga, Madagascar; kennedypasera@gmail.com
[2]Ph.D. Scholar, Laboratory of Applied Physics and Renewable Energies (LPADER), Ecole Doctorale Génie du Vivant et Modélisation (EDGVM), University of Mahajanga, Madagascar; zbenharith16@yahoo.com
[3]Professor, Laboratory of Applied Physics and Renewable Energies (LPADER), Ecole Doctorale Génie du Vivant et Modélisation (EDGVM), University of Mahajanga, Madagascar; bvdno2@gmail.com
Corresponding Author: PASERA Joanès Keneddy. E-mail: kennedypasera@gmail.com

Abstract: This study introduces a novel architecture of a dual-fluid photovoltaic–thermal (PVT) hybrid solar system equipped with fins, integrating a compound parabolic cylindrical concentrator, a dual-mode cooling system (water and air), a Maximum Power Point Tracking (MPPT) algorithm based on the Perturb and Observe (P&O) method, a Buck-Boost converter, and battery storage. The objective is to maximize the conversion of solar energy into both electricity and heat, while ensuring a reliable and autonomous energy supply for the needs of the LPADER university laboratory in Mahajanga. The methodology is based on rigorous mathematical modeling and numerical simulations performed in MATLAB, taking into account the local climatic conditions. The results highlight the potential of this architecture to ensure stable electrical generation, while efficiently recovering heat for domestic or agricultural applications. The dual-fluid CPVT hybrid field thus represents a sustainable and high-performance solution for decentralized electrification, particularly in rural areas or regions with unstable grids, thereby contributing to local sustainable development.

Keywords: Solar irradiation, Dual-fluid PVT, Fin, Parabolic cylindrical, MPPT, Buck-Boost, Performance

I. INTRODUCTION

la As in many countries around the world, Madagascar faces a strong dependence on fossil fuels, particularly hydrocarbons, which represents a major energy challenge. This dependency leads to critical consequences such as frequent power outages, a continuous increase in energy costs, and heightened vulnerability in the absence of sustainable alternative solutions [1]. In this context, the development of renewable energy has become an urgent necessity.

Madagascar possesses significant natural resource potential, particularly solar energy, benefiting from abundant sunlight throughout the year. Harnessing this renewable resource represents a strategic opportunity to meet the country's energy needs [2]. However, the efficiency of photovoltaic (PV) systems remains limited, mainly due to the overheating of solar cells, which significantly reduces their performance. This limitation justifies the use of hybrid technologies and advanced cooling strategies.

Among promising approaches, such as photovoltaic (PV) solar fields and concentrated photovoltaic (CPV) fields [3], dual-fluid concentrated photovoltaic–thermal (CPVT) systems stand out for their ability to simultaneously generate electricity and heat [4].

International Journal of Progressive Sciences and Technologies (IJPSAT)
ISSN: 2509-0119.

https://ijpsat.org/
Vol. 53 No. 1 October 2025, pp. 378-395

Building upon previous research, the dual-fluid CPVT system represents a more integrated and versatile solution for the optimized utilization of solar energy. The integration of a solar concentrator into a dual-fluid PVT system (using both water and air as heat transfer fluids) enhances thermal energy recovery while maintaining high electrical efficiency. This configuration thus constitutes an advanced technological solution to maximize the high-efficiency exploitation of solar energy.

The objective of this study is to analyze and optimize the energy performance of a dual-fluid CPVT concentrator system for efficient and autonomous electricity production. The proposed system is equipped with a Maximum Power Point Tracking (MPPT) algorithm coupled with a buck–boost converter and battery storage to reliably supply the energy demand of a university laboratory (LPADER). Beyond electricity generation, the system also enables the efficient use of recovered heat: hot water can be used for domestic or industrial purposes (heating, hot water supply), while hot air can serve for agricultural product drying, thereby improving overall energy efficiency.

The adopted methodology is based on rigorous mathematical modeling of each component, followed by comprehensive simulations in MATLAB to evaluate the system's performance under local climatic conditions. This study demonstrates the feasibility and advantages of such a solution for sustainable energy development in Mahajanga.

II. MATERIAL AND METHODS

2.1. Description de la configuration du système examine

The dual-fluid PVT hybrid collector is composed of several layers: a top glazing, photovoltaic (PV) cells, an EVA film, a Tedlar sheet, an upper absorber equipped with longitudinal rectangular fins, a network of parallel tubes carrying water and embedded within the air circulation chamber, a lower absorber, and thermal insulation. The collector is positioned between two symmetrical compound parabolic cylindrical concentrators, enabling the capture of both direct and reflected solar radiation. These reflectors focus solar energy onto the collector, thereby increasing the received irradiation and improving overall efficiency.

The PV cells generate electricity, while part of the solar radiation is converted into heat. This thermal energy is recovered by the heat transfer fluids circulating beneath the module [5]:

- Hot water is stored for thermal uses (heating, sanitary hot water).
- Hot air is directed to a drying chamber through a fan, ensuring uniform heat distribution for efficient product drying

A dual-fluid CPVT system has been designed to form a hybrid solar field. In the framework of this study, the field will consist of several CPVT units interconnected in series and parallel configurations:

- The thermal circuit (water/air) is connected in parallel.
- The electrical circuit is connected in a mixed (series/parallel) configuration to optimize voltage and current

A Maximum Power Point Tracking (MPPT) control adjusts in real time the load connected to the PV generator in order to maximize the extracted power, regardless of solar irradiance or temperature conditions [6],[7].

The Buck–Boost converter plays a key role in regulating the voltage and current delivered by the CPVT field. It dynamically adapts the generator's output to match the levels required by downstream devices, particularly:

- The battery, which stores energy for later use.
- The inverter, which requires a stable input voltage.

The converter thus enables adjustment of the output voltage (either higher or lower than the input), ensuring compatibility with the specifications of both the battery and the inverter. In case of low solar irradiation, an auxiliary thermal system powered by alternating current can be activated to maintain the desired drying temperature.

The energy stored in the battery supplies the inverter, ensuring continuous electricity delivery even in the absence of sunlight. The DC–AC inverter converts the energy from the CPVT field or the battery into alternating current to power electrical loads.

International Journal of Progressive Sciences and Technologies (IJPSAT)
ISSN: 2509-0119.

https://ijpsat.org/
Vol. 53 No. 1 October 2025, pp. 378-395

Figure 1 illustrates the architecture of the dual-fluid hybrid CPVT solar field, integrating the MPPT controller, Buck–Boost converter, battery, inverter, and loads.

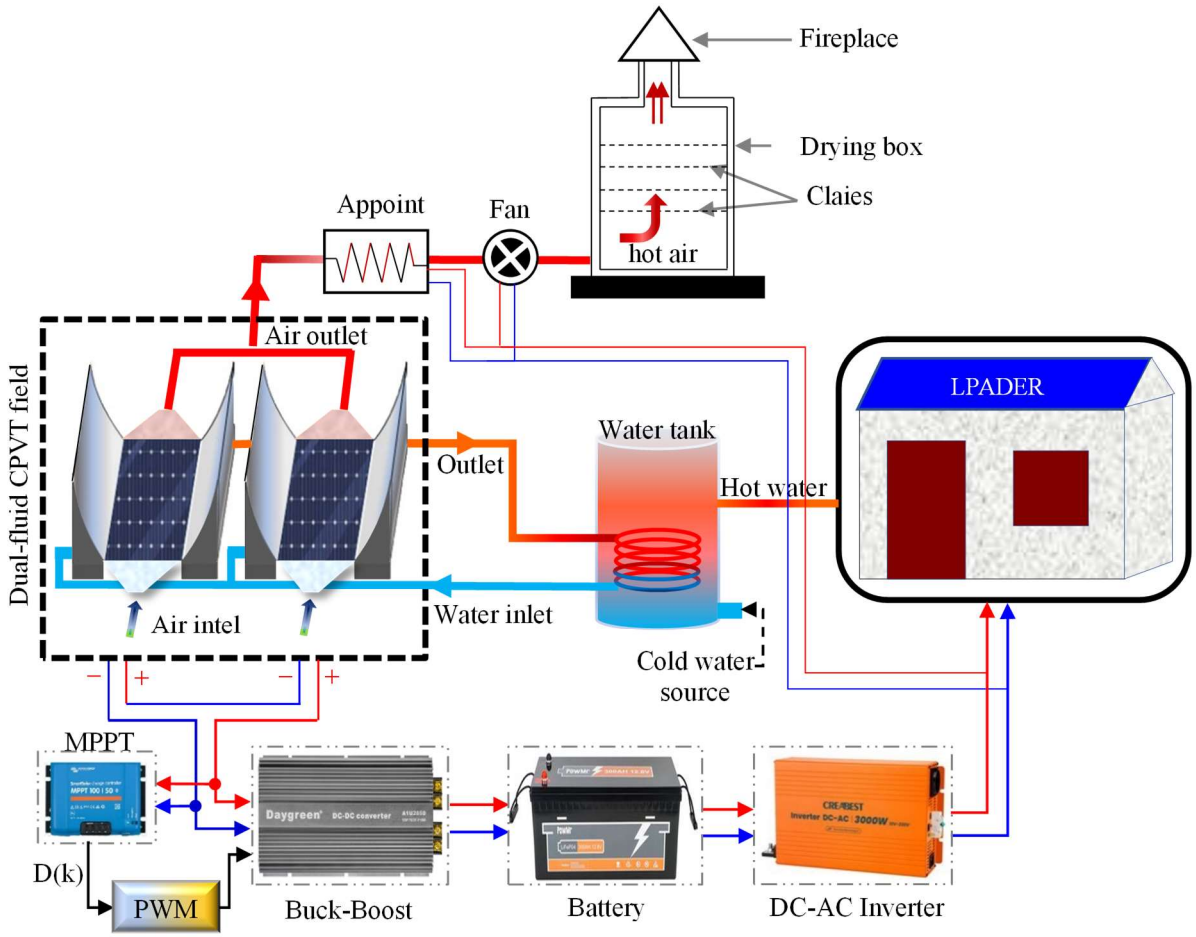

Figure 1. Système configuration dual-fluid CPVT field solar

A cross-section of a dual-fluid hybrid CPVT solar collector is shown in figure 2 [4],[8].

International Journal of Progressive Sciences and Technologies (IJPSAT)
ISSN: 2509-0119.

https://ijpsat.org/
Vol. 53 No. 1 October 2025, pp. 378-395

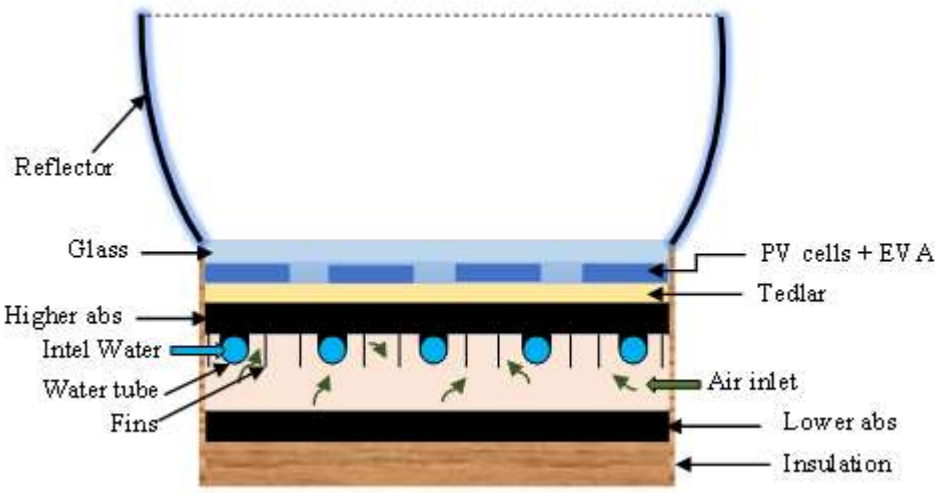

Figure 2. Front view sketch of dual-fluid CPVT system

2.2 Mathematical modeling

2.2.1 Study hypothesis

The mathematical models used to simulate the dual-fluid CPVT system are based on the following assumptions [4],[8],[9],[10]:

- The sky can be assimilated to a black body with an equivalent temperature calculated;
- Heat transfer is considered to be one-dimensional through the layers of the system;
- The ambient temperature is the same around the sensor;
- The floor temperature is taken to be equal to the ambient temperature;
- EVA's transmission coefficient is 100%;
- The ohmic losses of the solar cells are neglected;
- The mass flow rate is uniform in the air layer duct;
- Fluid flow in the tubes is assumed to be uniform;
- The wind speed on the face of the collector is assumed to be constant;
- The thermo-physical properties of water and air vary with temperature;
- The thermal and geometric properties of the two absorbers are equal;
- The thermal properties of the fins and tubes are equal to those of the absorber;
- The effect of shading and dust on the collector is negligible;
- The batteries are assumed to be fully charged as supplied by the manufacturer
- Self-discharge and aging phenomena have not been taken into account.

2.2.2 Equation the system

The mathematical model of the dual-fluid CPVT system is formulated based on energy balance equations applied to the individual control volumes, as presented in references [5],[8],[9],[10],[11],[12],[13],[14]:

Node 1 : outer face of glass

$$m_g Cp_g\left(\frac{dT_{g,ext}}{dt}\right) = A_g G_i C - h_{g-a}^{conv} A_g \left(T_{g,ext} - T_a\right) - h_g^{cond} A_g \left(T_{g,ext} - T_{g,int}\right) - h_{g-sky}^{rad} A_g \left(T_{g,ext} - T_{sky}\right) \quad (1)$$

Node 2 : inner face of glass pane

International Journal of Progressive Sciences and Technologies (IJPSAT)
ISSN: 2509-0119.

https://ijpsat.org/
Vol. 53 No. 1 October 2025, pp. 378-395

$$m_g Cp_g \left(\frac{dT_{g,int}}{dt}\right) = A_g \alpha_g G_i C + h_g^{cond} A_g \left(T_{g,ext} - T_{g,int}\right) - h_{g-cel}^{cond} A_g \left(T_{g,int} - T_{cel}\right) \quad (2)$$

Node 3 : PV cell

$$m_{cel} Cp_{cel} \left(\frac{dT_{cel}}{dt}\right) = A_{cel} \tau_g \alpha_{cel} G_i C + h_{g-cel}^{cond} A_{cel} \left(T_{g,int} - T_{cel}\right) - h_{cel-ted}^{cond} A_{cel} \left(T_{cel} - T_{ted}\right) - Q_{élec} \quad (3)$$

Node 4 : tedlar layer

$$m_{ted} Cp_{ted} \left(\frac{dT_{ted}}{dt}\right) = h_{cel-ted}^{cond} A_{ted} \left(T_{cel} - T_{ted}\right) - h_{ted-absh}^{cond} A_{ted} \left(T_{ted} - T_{absh}\right) \quad (4)$$

Node 5 :top absorber layer

$$\begin{aligned} m_{abs} Cp_{abs} \left(\frac{dT_{absh}}{dt}\right) &= h_{ted-absh}^{cond} A_{abs} \left(T_{ted} - T_{absh}\right) - h_{absh-air}^{conv} A_{absh-air} \left(T_{absh} - T_{air}\right) - U_{fin} \left(T_{absh} - T_{air}\right) \\ &\quad - h_{absh-tube}^{cond} A_{absh-tube} \left(T_{absh} - T_{tube}\right) - h_{absh-absl}^{rad} A_{absh-absl} \left(T_{absh} - T_{absl}\right) \end{aligned} \quad (5)$$

With [4],[14]: $U_{fin} = h_{absh-air}^{conv} . \eta_{fin} . A_{absh-air}$ (6)

$$\eta_{fin} = \frac{\tanh\left(L_c \cdot \sqrt{\frac{P.h_{fin}^{conv}}{\lambda_{fin} e_{fin}}}\right)}{L_c \cdot \sqrt{\frac{P.h_{fin}^{conv}}{\lambda_{fin} . e_{fin}}}}, \quad A_{absh-air} = N.\left(2.H_{fin} . L_c\right) + A_{absh} + A_{tube}, \quad L_c = L + \frac{e_{fin}}{2} \text{ and } P = 2\left(L + e_{fin}\right) \quad (7)$$

Where : $A_{absh-air}$, L_c, P and e_{fin} are respectively the total available area, corrected length, perimeter and thickness of a fin.

Node 6 : tube layer

$$\begin{aligned} m_{tube} Cp_{tube} \left(\frac{dT_{tube}}{dt}\right) &= h_{absh-tube}^{cond} A_{absh-tube} \left(T_{absh} - T_{tube}\right) - h_{tube-wat}^{conv} A_{tube-wat} \left(T_{tube} - T_{wat}\right) \\ &\quad - h_{tube-air}^{conv} A_{tube-air} \left(T_{tube} - T_{air}\right) - h_{tube-absl}^{ray} A_{tube-absl} \left(T_{tube} - T_{absl}\right) \end{aligned} \quad (8)$$

Node 7 **:**heat transfer fluid water

$$m_{wat} Cp_{wat} \left(\frac{dT_{wat}}{dt}\right) = h_{tube-wat}^{conv} A_{tube-wat} \left(T_{tube} - T_{wat}\right) - \dot{m}_{wat} Cp_{wat} \left(T_{wat,out} - T_{wat,int}\right) \quad (9)$$

Node 8:heat transfer fluid air

$$\begin{aligned} m_{air} Cp_{air} \left(\frac{dT_{air}}{dt}\right) &= h_{absh-air}^{conv} A_{absh-air} \left(T_{absh} - T_{air}\right) + h_{air-absl}^{conv} A_{air-absl} \left(T_{absl} - T_{air}\right) \\ &\quad + h_{tube-air}^{conv} A_{tube-air} \left(T_{tube} - T_{air}\right) + U_{fin} \left(T_{absh} - T_{air}\right) - \dot{m}_{air} Cp_{air} \left(T_{air,out} - T_{air,int}\right) \end{aligned} \quad (10)$$

International Journal of Progressive Sciences and Technologies (IJPSAT)
ISSN: 2509-0119.

https://ijpsat.org/
Vol. 53 No. 1 October 2025, pp. 378-395

Node 9 :lower absorber layer

$$m_{absl}Cp_{absl}\left(\frac{dT_{absl}}{dt}\right)=h^{conv}_{air-absl}A_{air-absl}\left(T_{air}-T_{absl}\right)+h^{rad}_{absh-absl}A_{absh-absl}\left(T_{absh}-T_{absl}\right)+h^{rad}_{tube-absl}A_{tube-absl}\left(T_{tube}-T_{absl}\right)-h^{cond}_{absl-is}A_{absl-is}\left(T_{absl}-T_{is,int}\right) \quad (11)$$

Node 10 : inner face of the insulation

$$m_{is}Cp_{is}\left(\frac{dT_{is,int}}{dt}\right)=h^{cond}_{absl-is}A_{is}\left(T_{absl}-T_{is,int}\right)-h^{cond}_{is}A_{is}\left(T_{is,int}-T_{is,ext}\right) \quad (12)$$

Node 11 :outer face of the insulation

$$m_{is}Cp_{is}\left(\frac{dT_{is,ext}}{dt}\right)=h^{cond}_{is}A_{is}\left(T_{is,int}-T_{is,ext}\right)-h^{conv}_{is-a}A_{is}\left(T_{is,ext}-T_{a}\right)-h^{rad}_{is-sol}A_{is}\left(T_{is,ext}-T_{sol}\right) \quad (13)$$

The physical properties of air are assumed to vary linearly with temperature, in accordance with the relations established by Ebrahim and Alfege [4], [5], [10].

The thermophysical properties of water are likewise considered to vary linearly with temperature [4],[8],[15],[16],[17].

A comprehensive description of all mathematical models is available in [4], [8].

2.2.3 Compound Parabolic Cylindrical Solar Concentrator [11],[18],[19], [20]

The compound parabolic cylindrical concentrator is an advancement of the simple parabolic trough concentrator, providing improved solar radiation capture and a more homogeneous distribution of energy over the dual-fluid PVT receiver. This reduces hot spots and enhances both the thermal and optical efficiency of the system. The energy concentration of a solar collector is defined as the ratio between the solar energy intercepted by the concentrator aperture and the energy actually received by the dual-fluid PVT receiver. It depends on the optical efficiency and the geometric concentration factor [4], [8].

$$C_e = C_g \times \eta_{opt} = \left(1/\sin\left(\theta_a\right)\right)\times\left(\rho_{ccp}\right)^{N_r}\times\eta_{int} \text{ with } \eta_{int}=1-e^{-C_g} \quad (14)$$

Where : θ_a , ρ_{ccp} , N_r et η_{int} denote the acceptance angle, the mirror reflectivity, the average number of reflections experienced by a ray before reaching the dual-fluid PVT receiver, and the intercept factor, respectively.

2.2.4 Electrical model of a dual-fluid PVT system

The electrical behavior of the PVT system is strongly influenced by the intensity of solar irradiation and the temperature of the photovoltaic cells. For a single-diode model, the expression for the electric current leaving the photovoltaic collector is written as follows [9],[21] :

$$I_{PV}=N_p.I_{ph}-N_p.I_0\left[\exp\left(q\frac{V_{PV}+I_{PV}.R_S}{n.N_S.K.T}\right)-1\right]-\frac{V_{PV}+I_{PV}.R_S}{R_{sh}} \quad (15)$$

Where: I_{ph}, I_0, R_s, R_{sh}, q, N_s, N_p, n and K are respectively photon current, diode saturation current, series resistance, parallel resistance, electron charge, number of cells in series, number of cells in parallel, ideality factor, Boltzmann constant.

Current and voltage values vary with solar irradiation intensity and cell temperature, as shown in the following equations [8],[9],[21]:

International Journal of Progressive Sciences and Technologies (IJPSAT)
ISSN: 2509-0119.

https://ijpsat.org/
Vol. 53 No. 1 October 2025, pp. 378-395

- Output current variation: $I(G_i C, T_{cel}) = I_{ref} + \Delta I = I_{ref} + k_i \left(\frac{G_i C}{G_{ref}}\right)\Delta T + \left(\frac{G_i C}{G_{ref}} - 1\right) I_{sc,ref}$ (16)
- Output voltage variation: $V(G_i C, T_{cel}) = V_{ref} + \Delta V = V_{ref} + k_v \cdot \Delta T - R_S \cdot \Delta I$ (17)
- Short-circuit current variation: $I_{sc}(G_i C, T_{cel}) = \left(\frac{G_i C}{G_{ref}}\right) \times \left(k_i \cdot \Delta T + I_{sc,ref}\right)$ (18)
- Short-circuit current variation: $V_{oc}(G_i C, T_{cel}) = V_{oc,ref} + k_v \cdot \Delta T + n \cdot \ln\left(\frac{G_i C}{G_{ref}}\right)$ (19)

With: $\Delta T = T_{cel} - T_{ref}$ (20)

Where k_i and k_v are respectively the coefficient of variation of current and voltage as a function of temperature.

2.2.5 Performance of the PVT dual-fluid hybrid collector

The electrical power and thermal power produced by the PVT dual-fluid hybrid solar collector are given by the following equations [4],[5],[9],[22],[23] :

$$Q_{élec} = \tau_g . G_i . C . S_{cell} . \eta_{ref} . \exp\left[\beta\left(T_{cel} - T_{ref}\right)\right], \text{ where } G_i \text{ is the global solar irradiance.} \quad (21)$$

$$Q_{the,wat} = \dot{m} . Cp_{wat} . \left(T_{wat,out} - T_{wat,int}\right) \text{ and } Q_{the,air} = \dot{m} . Cp_{air} . \left(T_{air,out} - T_{air,int}\right) \quad (22)$$

$$Q_{the,PVT\_bi-fluid} = Q_{the,wat} + Q_{the,air} \quad (23)$$

The electrical and thermal efficiencies of the PVT dual-fluid hybrid solar collector are determined by the following two expressions [24],[25],[26] :

$$\eta_{elc} = \frac{Q_{elec}}{S_{cel} \cdot G_i \cdot C} \text{ and } \eta_{the,PVT\_bi-fluid} = \frac{Q_{the,PVT\_bi-fluid}}{S_{cel} \cdot G_i \cdot C} \quad (24)$$

The overall efficiency of a dual-fluid PVT is the sum of the thermal efficiency and the thermal efficiency equivalent to the electrical efficiency [24],[25],[26],[27]:

$$\eta_{PVT\_bi-fluid} = \eta_{the} + \eta_{elec,the} \text{ ; with : } \eta_{elec,the} = \frac{\eta_{elec}}{C_f}, \quad (25)$$

Where C_f represents the thermal energy conversion factor, with a typical value of 0.38 [27].

2.2.7 Buck–Boost Converter Modeling

To derive the mathematical model of the converter, it must be analyzed in its two operating phases (switch closed and switch open) by applying Kirchhoff's laws to the corresponding equivalent circuits [28],[29],[30].

During the first interval D·T, the switch k is closed during the second interval (1−D)·T, the switch k is open.

International Journal of Progressive Sciences and Technologies (IJPSAT)
ISSN: 2509-0119.

https://ijpsat.org/
Vol. 53 No. 1 October 2025, pp. 378-395

$$\begin{cases} I_{C_1}(t) = C_1 \dfrac{dV_{PVT}(t)}{dt} = I_{PVT}(t) - I_L(t) \\ I_{C_2}(t) = C_2 \dfrac{dV_{out}(t)}{dt} = -I_{out}(t) \\ V_L(t) = L \dfrac{dI_L}{dt} = V_{PVT}(t) \end{cases} \quad (26) \qquad \begin{cases} I_{C_1}(t) = C_1 \dfrac{dV_{PVT}(t)}{dt} = I_L(t) \\ I_{C_2}(t) = C_2 \dfrac{dV_{out}(t)}{dt} = I_L(t) - I_{out}(t) \\ V_L(t) = V_{PVT}(t) - V_{out}(t) \end{cases} \quad (27)$$

Rearranging the terms of the previous equations yields the dynamic model of the buck-boost converter:

$$\begin{cases} I_L(t) = \dfrac{1}{D}\left(I_{PVT} - C_1 \dfrac{dV_{PVT}(t)}{dt} \right) \\ I_{out}(t) = -(1-D).I_L(t) - C_2 \dfrac{dV_{out}(t)}{dt} \\ V_{PVT}(t) = \dfrac{1}{D}\left(-(1-D)V_{out}(t) + L \dfrac{dI_L(t)}{dt} \right) \end{cases} \quad (29), \quad \begin{cases} V_{out}(t) = \dfrac{D}{(1-D)} V_{PVT}(t) \\ I_{out}(t) = \dfrac{(1-D)}{D} I_{PVT}(t) \end{cases} \quad (30) \quad \text{and} \quad \begin{cases} R_{eq} = R_{batt}\left(\dfrac{1-D}{D} \right)^2 \\ D = \dfrac{V_{out}}{V_{PVT} + V_{out}} \end{cases} \quad (31)$$

The component values to be selected are determined as follows [30]:

$$L = \frac{D.V_{PVT}}{f.\Delta I_L} \ , \ C_1 = \frac{I_{PVT} - D.I_L}{2.\Delta V_{PVT}} \text{ and } C_2 = \frac{D^2.V_{PVT}}{(1-D).f.R_{batt}.\Delta V_{out}} \quad (32)$$

Where: $D, f, \Delta I_L, \Delta V_{out}, R_{eq}$ represent, respectively, the duty cycle, the switching frequency, the inductor current ripple, the output voltage ripple across the capacitor, and the equivalent load reflected by the boost converter as seen from the PV side.

2.2.6 Algorithme de commande P&O

Figure 3 illustrates the Perturb and Observe (P&O) MPPT control algorithm [31]

International Journal of Progressive Sciences and Technologies (IJPSAT)
ISSN: 2509-0119.

https://ijpsat.org/
Vol. 53 No. 1 October 2025, pp. 378-395

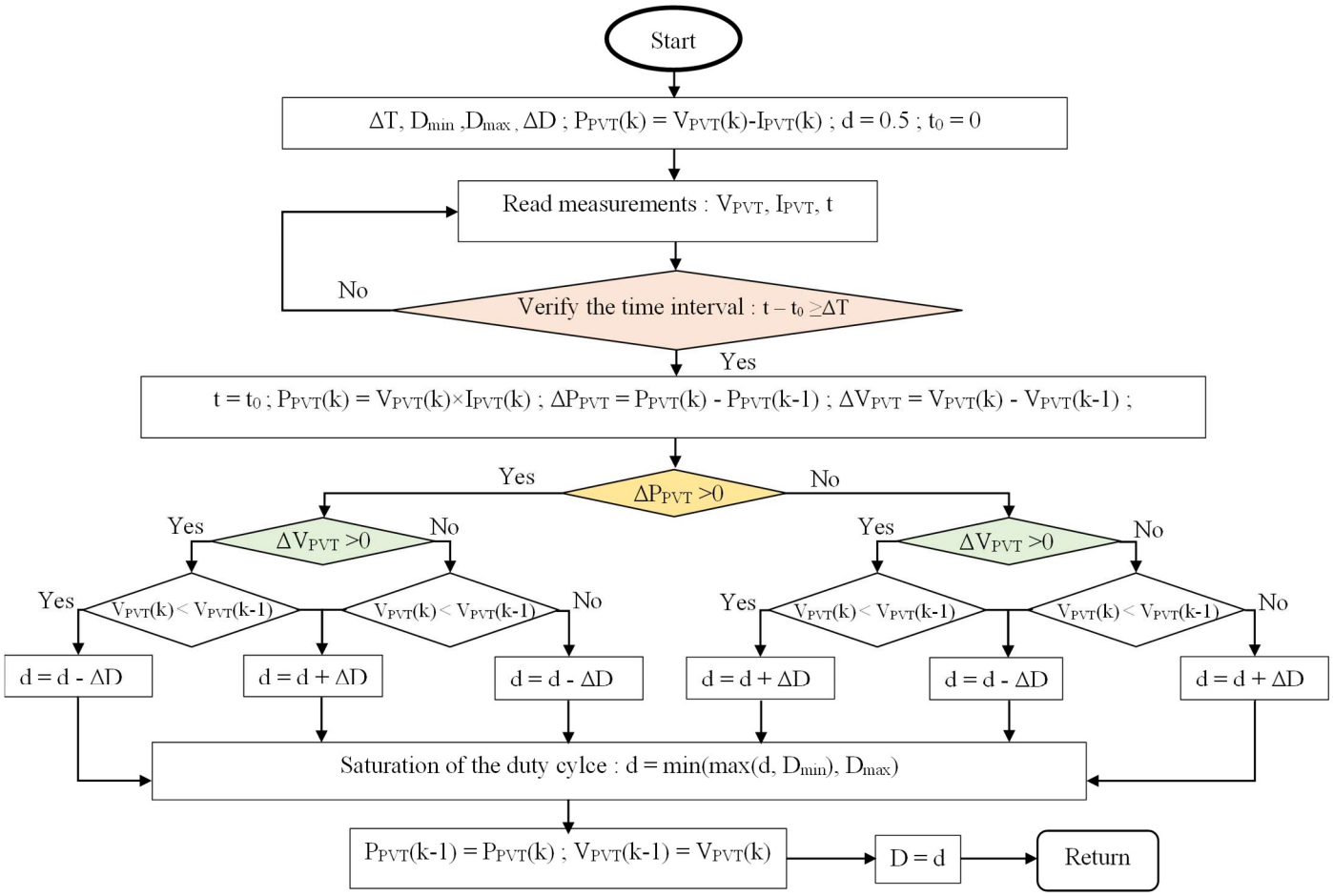

Figure 3. MPPT algorithm based on P&O method

2.2.8 Battery charge modeling

Battery charge modeling involves determining the energy required to recharge the battery after a period of discharge [32],[33].

- Energy required by the load (kWh): $E_{ch} = P_{ch} \times t$ (33)
- Energy supplied by the battery to the inverter: $E_{batt,inver} = \frac{E_{ch}}{\eta_{inver}}$ (34)
- Usable and actual capacity (Ah): $C_{utile} = \frac{E_{batt} \times 1000}{V_{batt}}$, and $C_{reel} = \frac{C_{utile}}{DOD}$ (35)
- Recharge time (h): $t_{rech} = \frac{E_{batt}}{Q_{elec} \times \eta_{mppt} \times \eta_{conv} \times \eta_{ch\_batt}}$ (36)
- Discharge time: $t_{dech} = \frac{C_{total\_batt} \times DOD \times V_{total\_batt} \times \eta_{dech} \times \eta_{inver}}{1000 \times P_{ch}}$ (37)
- Overall efficiency : $\eta_{tolat} = \eta_{PVT} . \eta_{conv} . \eta_{mppt} . \eta_{inver}$ (38)

International Journal of Progressive Sciences and Technologies (IJPSAT)
ISSN: 2509-0119.

https://ijpsat.org/
Vol. 53 No. 1 October 2025, pp. 378-395

Where: $C_{total\_batt} = N_{parl} \times C_{batt\_unité}$ and $V_{total\_batt} = N_{serie} \times V_{batt\_unité}$ (39)

Where P_{ch} , η_{inver} , E_{batt} , DOD, V_{total_batt} : are respectively the total power of the load, conversion efficiency (inverter), energy actually available in the battery, depth of discharge allowed, and total voltage available in the system (battery).

2.3 Study site

The data used were obtained from the ASECNA meteorological station in Mahajanga, located in the northwestern region of Madagascar (15°43' S, 46°19' E). The Page model was employed to estimate solar irradiation based on insolation data collected between 2010 and 2024.

2.4 Electrical characteristics

The polycrystalline silicon photovoltaic collector described in Table 1 has been evaluated to international standards at 1000 $W.m^{-2}$, AM 1.5 and 25°C.

Table 1: Electrical characteristics of a KC200GT photovoltaic module [4],[21],[34].

Experimental peak power P_{max}	200 W
Voltage at point of maximum power V_{pm}	26.3 V
Current at point of maximum power I_{pm}	7.61 A
Open circuit voltage V_{oc}	32.9 V
Short-circuit current I_{sc}	8.21 A
Voltage temperature coefficient k_v	–0.123 V/°C
Current temperature coefficient k_i	0.00318 A/°C
Operating temperature	–40 °C to +85 °C
Number of cells in series N_s	54
Number of parallel cells N_p	1
Reference yield	15%
Dimensions $(L \times l \times h)$	1425 mm × 990 mm × 36 mm

Table 2 illustrates the electrical characteristics of Titan Lithium Iron Phosphate (LiFePO4) batteries.

Table 2: Electrical performance [35]

Voltage range	58.4 V – 43.2 V
Nominal Capacity	300 Ah
Maximum charging current	150 A
Maximum discharge current	200 A

Table 3 shows the electrical characteristics of the Quattro inverter (48V/10000VA – 230V).

Table 3: Electrical characteristics of a Quattro inverter [36]

Supply voltage range	37.2 – 68 V
Output	Output voltage: 230 VAC ± 2% 50Hz or 60 Hz ± 0.1 %
Maximum efficiency 12/24/48V (%)	95 / 96%

International Journal of Progressive Sciences and Technologies (IJPSAT)
ISSN: 2509-0119.

https://ijpsat.org/
Vol. 53 No. 1 October 2025, pp. 378-395

2.5 Component characteristics of the PVT dual-fluid hybrid module

Table 4 shows the characteristics of the various sensor components.

Table 4. Characteristics of the PVT dual-fluid hybrid collector components [4],[9],[10],[22].

Components / Features	Glass	PV cell	Tedlar	Absorber	Tube	Insulation	Unit
Density	2200	2330	1300	2700	2700	60	($kg \cdot m^{-3}$)
Specific heat	670	836	1400	900	900	700	($J.^{kg-1K-(1}$)
Thermal conductivity	0.93	148	0.033	237	237	0.04	(W. $^{K-1}.^{m-1}$)
Emissivity	0.88	0.93	0.88	0.04	0.04	0.85	---
Thickness	0.003	0.0003	0.0005	0.005	0.001	0.004	(m)
Absorption coefficient	0.066	0.85	0.5	0.75	0.75	0.066	---
Pipe outside diameter					0.014		(m)
Inside pipe diameter					0.012		(m)

2.6 LPADER load

For the daily requirements of the LPADER, the table below presents the amount of energy needed to meet the demand.

Table 5. LPADER energy requirements

Equipment	Quantity	Nominal power (W)	Power (W)	Usage (hours)	Daily consumption (kWh/day)
Long lamp	2	20	40	12	480
LED bulb	2	13	26	5 to 8	130 to 260
Video projector	1	1000	100	5 to 8	5000 to 8000
Desktop computer	10	300	30	5 to 15	12,000 to 28,800
500 L refrigerator	1	150	150	20	3600
Oscilloscope	1	70	70	5	350
Printer	1	40	40	5 to 8	200 to 320
Fan	2	60	120	10	1200
Total			**3846**		**21.16 to 58.56**

International Journal of Progressive Sciences and Technologies (IJPSAT)
ISSN: 2509-0119.

https://ijpsat.org/
Vol. 53 No. 1 October 2025, pp. 378-395

III. RESULTS AND DISCUSSION

3.1 Variation of solar irradiation and ambient temperature in Mahajanga

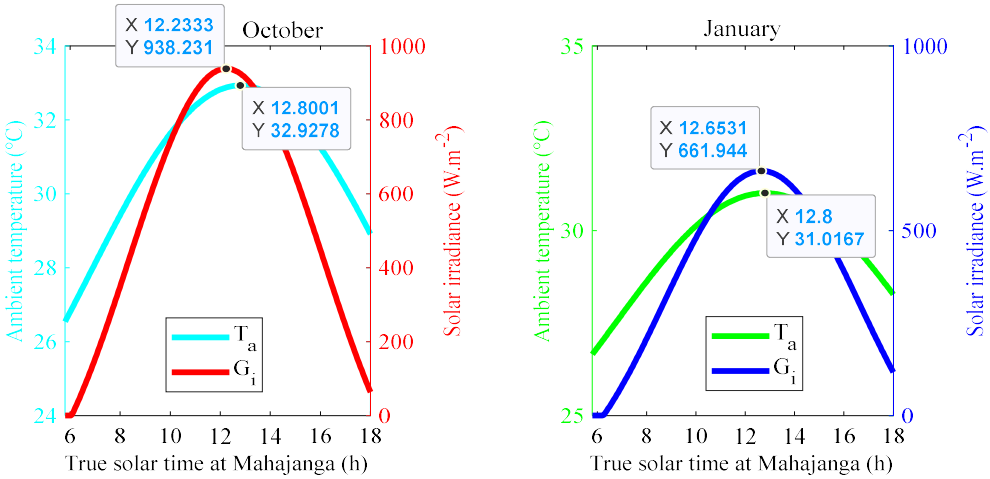

Figure 4. Temporal variation of solar irradiation and ambient temperature in Mahajanga

Figure 4 presents the simulated evolution of the monthly average solar irradiation and ambient temperature over a typical day of the considered month, based on a 14-year dataset (2010–2024).

In October, solar irradiation gradually increases from sunrise, reaching a peak of 938 W.m^{-2} around 12:14 p.m., before steadily decreasing until sunset. The ambient temperature follows a slightly shifted curve due to thermal inertia, with a maximum of 32.9 °C reached at approximately 12:48 p.m., i.e., about half an hour after the irradiation peak. It is also observed that the morning temperature is lower than that of the afternoon, illustrating the thermal accumulation effect throughout the day.

In January, a similar trend is observed, although with slightly different values. The maximum irradiation reaches 661.9 W.m^{-2} at 12:39 p.m., which represents a significant decrease compared to October, likely due to higher cloud coverage or a less favorable solar angle. The maximum ambient temperature is recorded at 31 °C around 12:48 p.m., also slightly shifted with respect to the irradiation peak.

These results emphasize the importance of considering both solar irradiation and thermal evolution in the design and sizing of CPVT systems, particularly to optimize thermal recovery in accordance with the actual solar hours.

International Journal of Progressive Sciences and Technologies (IJPSAT)
ISSN: 2509-0119.

https://ijpsat.org/
Vol. 53 No. 1 October 2025, pp. 378-395

3.2 Energy Performance of the Dual-Fluid CPVT System

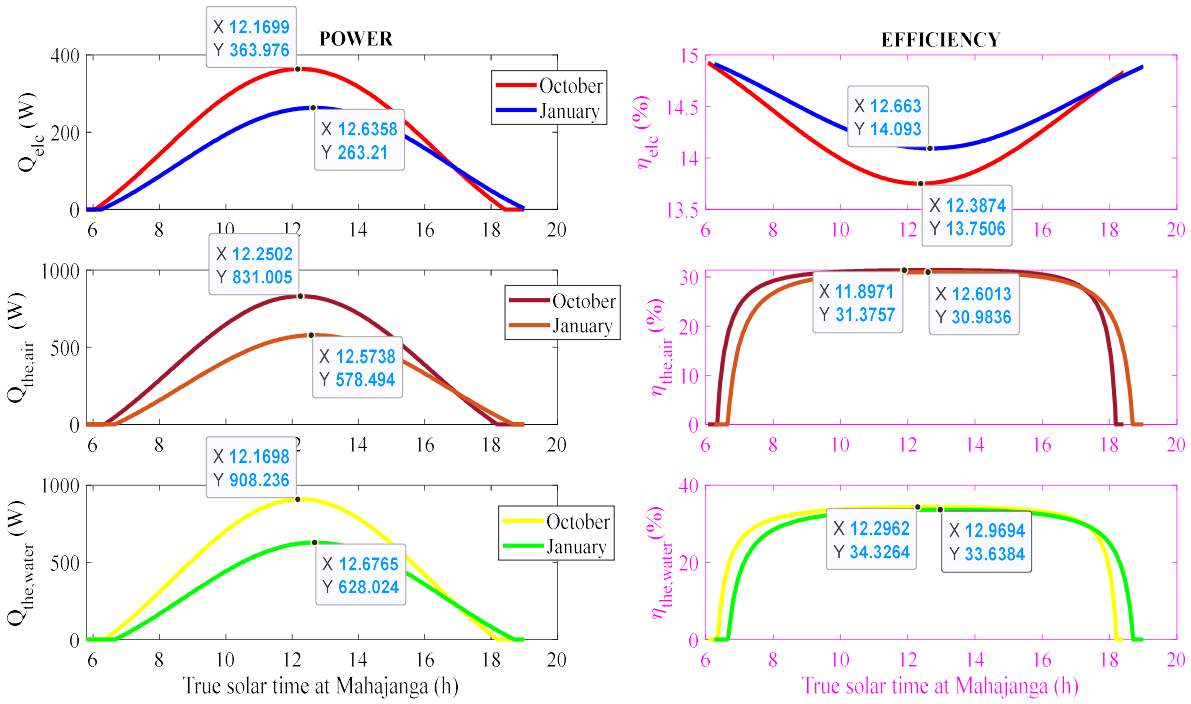

Figure 5. Electrical and thermal performance of the dual-fluid CPVT system

Figure 5 highlights the remarkable overall efficiency of the dual-fluid CPVT system, achieved through carefully selected geometric and operational parameters under moderate solar concentration (C = 2). The optimal conditions include: 15 fins, 5 absorber tubes, a fin thickness of 0.03 m, a fin height of 0.025 m, an air gap of 0.03 m, a fin–tube spacing of 0.046 m, as well as mass flow rates of 0.016 kg.s^{-1} for water (per tube) and 0.022 kg.s^{-1} for air. These values were chosen to ensure a suitable compromise between heat transfer efficiency and system compactness.

The results demonstrate a remarkable thermal–electrical synergy between the two working fluids (air and water), enabling optimal utilization of the available solar energy. From the photovoltaic perspective, the electrical power output reaches a peak of 363.97 W around midday, with a maximum electrical efficiency of 13.75 %. This efficiency remains relatively stable during the period of strong solar irradiation (approximately between 10 a.m. and 2 p.m.), illustrating the ability of the system to maintain stable electrical conversion despite the temperature rise induced by solar concentration.

On the thermal side, the system also exhibits balanced and complementary performance between air and water. The thermal power extracted through air reaches a maximum of 831 W, while the thermal power associated with water amounts to 908.23 W, reflecting high effectiveness in heat recovery by both fluids. The observed thermal efficiencies are also high and relatively stable between 9 a.m. and 4 p.m., with peak values of 31.3 % for air and 34.32 % for water, demonstrating efficient thermal management during most of the solar day.

These results clearly demonstrate the potential of the optimized dual-fluid CPVT system for cogeneration applications (electricity + heat). Such a solution is particularly well-suited for autonomous or hybrid installations in sunny regions, where it can simultaneously supply electrical equipment while meeting thermal needs such as water heating, agricultural product drying, or other domestic uses. The balance achieved between electrical conversion and thermal recovery underlines the strategic interest of the dual-fluid approach, which maximizes solar spectrum exploitation while reducing heat losses.

International Journal of Progressive Sciences and Technologies (IJPSAT)
ISSN: 2509-0119.

https://ijpsat.org/
Vol. 53 No. 1 October 2025, pp. 378-395

3.3 Electrical Evolution of the Dual-Fluid CPVT System with MPPT and Buck-Boost Converter

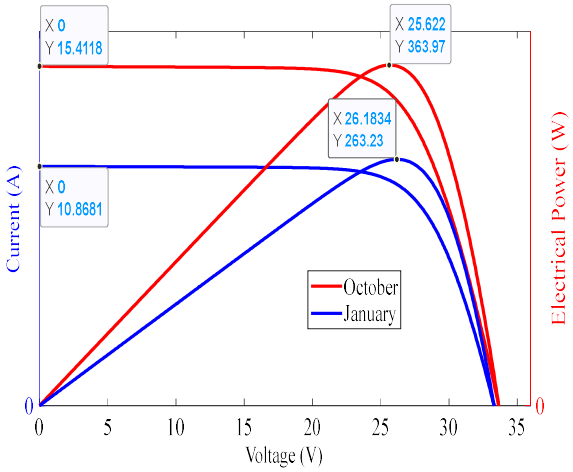

Figure 6. I-V-P characteristics of the dual-fluid CPVT system with MPPT

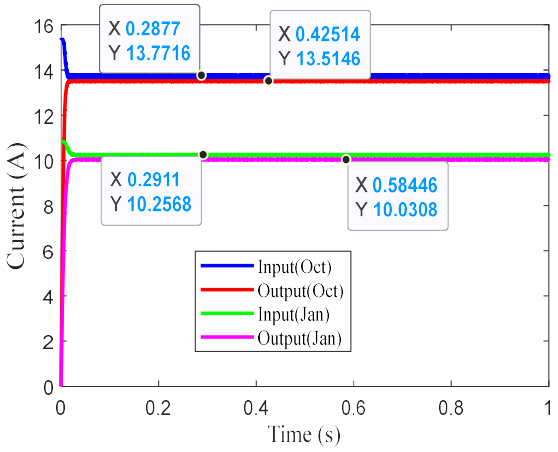

Figure 7. Current of the dual-fluid CPVT system with MPPT and Buck-Boost

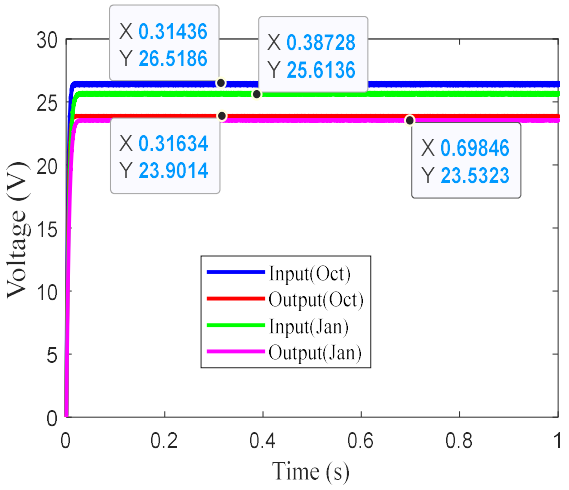

Figure 8. Voltage of the dual-fluid CPVT system with MPPT and Buck-Boost

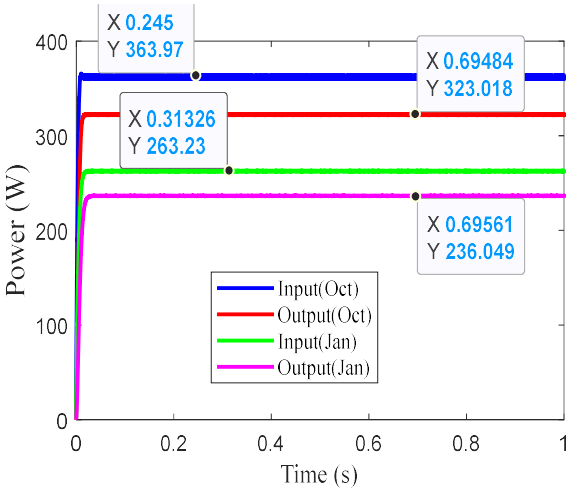

Figure 9. Power of the dual-fluid CPVT system with MPPT and Buck-Boost

Figures 6 to 9 illustrate the electrical performance of the dual-fluid CPVT system equipped with an MPPT algorithm and a Buck–Boost converter, for two representative periods in Mahajanga: October (high solar irradiation) and January (low solar irradiation). Figure 6 shows that the maximum power (Pmp) extracted reaches 363.87 W in October compared to 263.23 W in January, this difference being mainly attributed to higher solar irradiation. The short-circuit current (Isc) is also higher in October, confirming a greater energy capture. Conversely, the voltage at the maximum power point (Vmp) remains relatively stable, around 25.8 V in October and 26.18 V in January; this slight variation is attributed to the cell temperature, itself influenced by the ambient temperature: higher in October, it reduces the output voltage of the photovoltaic cells.

Figure 7 highlights the dynamic behavior of the current at the input and output of the converter: a fast rise (response time < 0.2 s) is observed, indicating a highly responsive system. The output current of the converter is lower than that of the dual-fluid CPVT, since the Buck–Boost converter adapts the output voltage (generally higher), which mechanically results in a reduction of the current in order to maintain power balance. The profile remains consistent between October and January, demonstrating stable operation.

International Journal of Progressive Sciences and Technologies (IJPSAT)
ISSN: 2509-0119.

https://ijpsat.org/
Vol. 53 No. 1 October 2025, pp. 378-395

Figure 8 shows that the input voltage is adjusted by the MPPT to track the maximum power point: in October, it is approximately 25.6 V at the input and 26.5 V at the output; in January, the voltages are slightly lower but remain stable. The MPPT dynamically regulates the voltage through duty cycle control of the converter, ensuring optimal power extraction despite climatic variations.

Finally, Figure 9 shows that the output power of the converter is slightly lower than the input power (363.97 W at the input versus 323.02 W at the output in October; 263.23 W versus 236.05 W in January), which corresponds to inherent conversion losses (about 10%) due to the electronic components and the inductance.

Overall, these figures confirm the efficiency of the system in both transient and steady-state regimes, with a fast response, absence of overshoot or overvoltage, consistent current management, and no excessive oscillations in the dynamic response. The system thus achieves stable power extraction, demonstrating the combined effectiveness of the MPPT algorithm and the Buck–Boost converter

3.4 Operation and Electrical Performance of a Hybrid Solar Field Combining a Dual-Fluid CPVT System and Battery Storage

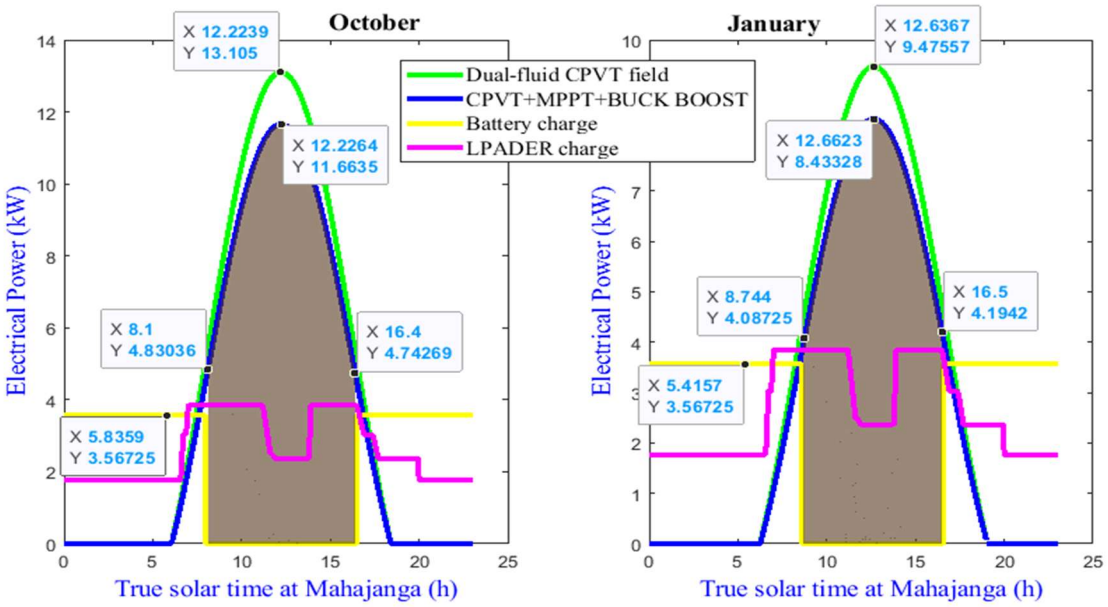

Figure 10. Temporal evolution of the electrical performance of the studied system on a typical day in October and January

Figure 10 illustrates the operation of a hybrid dual-fluid CPVT solar field in Mahajanga during two representative periods (October and January), integrating an MPPT algorithm with a Buck-Boost converter and a battery storage system.

The load profile of the LPADER laboratory at the University of Mahajanga varies according to the time of day and activity: low consumption during the night (1.7 kW), a sharp increase to 3.8 kW from 7:00 a.m., a drop to around 2.8 kW during off-peak hours (around 11:00 a.m.), followed by a rise to 3.8 kW at 2:00 p.m., and then a gradual decrease from 4:00 p.m. The battery bank, assumed to be fully charged, is sized to supply the load between 4:00 p.m. and 8:00 a.m., delivering 3.2 kW of usable power after inversion, corresponding to an autonomy of approximately 20 hours. From 8:00 a.m., the battery switches with the dual-fluid concentrated solar field, which simultaneously supplies the load and recharges the batteries.

The dual-fluide CPVT field, composed of 36 modules connected in series/parallel, reaches a maximum power of 13.1 kW (October) or 9.5 kW (January) without conversion, which decreases to 11.66 kW and 8.43 kW, respectively, after passing through the converter due to losses associated with the overall efficiency of the MPPT and Buck-Boost system. The main advantage of this converter lies in its ability to stabilize the output voltage and optimize energy extraction, despite the slight power reduction. The

system is designed to intelligently switch between the solar field and the battery, ensuring uninterrupted power supply to the laboratory, even during low-irradiance days.

Finally, the comparison between October and January shows lower solar power during the wet season, as well as a shift in the transition time between the battery and the dual-fluid CPVT field, although the overall operating principle remains unchanged. This shift is primarily due to variations in solar altitude and sunrise/sunset times, which change with the seasons.

IV. CONCLUSION

This work has proposed a new architecture and simulation of a dual-fluid CPVT (Concentrated Photovoltaic Thermal) hybrid solar system, designed to optimize the conversion of solar energy into both electricity and heat. The proposed system integrates a solar concentrator, dual-fluid cooling (water and air), a double absorber with fins on one side, a Buck–Boost converter, an MPPT algorithm based on the Perturb & Observe (P&O) method, as well as a battery storage unit. This configuration ensures stable, reliable, and fully autonomous energy production, tailored to the needs of the LPADER university laboratory.

The obtained results demonstrate the high performance of this cogeneration architecture. The system simultaneously produces electrical and thermal energy, with an overall efficiency more than twice that of a conventional photovoltaic field, with or without concentration. Under an irradiation of 938 $W.m^{-2}$, a power output of 13 kW was achieved with a reduced number of modules, confirming the effectiveness of the proposed optimization.

The integration of battery storage represents a key advantage: it ensures supply continuity despite solar irradiation fluctuations, thereby guaranteeing constant energy availability, even in isolated sites or regions with unstable grids. The system therefore provides an autonomous and intelligent electrification solution, while optimizing energy management.

The P&O MPPT algorithm proved effective for rapid and accurate tracking of the maximum power point, even under variable conditions. Moreover, the dynamic response of the Buck–Boost converter confirmed the system's stability, with no overshoot or oscillations, thereby validating the robustness of the entire device.

Thus, the dual-fluid CPVT system with storage constitutes a sustainable, high-performance energy solution adapted to the needs of decentralized electrification. It opens promising perspectives for energy autonomy in rural areas and developing countries, while valorizing the recovered heat for domestic or agricultural applications.

ACKNOWLEDGEMENTS

First and foremost, I would like to express my deepest gratitude to my thesis supervisor, Professor DONA Victorien Bruno, for his kind guidance, invaluable advice, and unwavering support throughout the preparation of this work. His scientific rigor, availability, and insight have been an invaluable source of inspiration. Thanks to his mentorship, I was able to make significant progress and develop both academically and personally.

I would also like to extend my sincere thanks to my fellow PhD student, HARITHI BEN Daoud Ben Attoumane for their valuable collaboration, stimulating discussions, and constant support. Their spirit of cooperation and the quality of our scientific exchanges greatly enriched my thinking and strengthened my motivation throughout this research.

Finally, I would like to express my heartfelt gratitude to my daughters, PASERA Eindjy Kheira and PASERASOA Airah Kanssi, for their love, patience, and constant encouragement, which have been a source of strength and motivation throughout my doctoral journey.

REFERENCES

[1] Minh HUYNH QUANG, Optimisation de la production de l'électricité renouvelable pour site isolé, Thèse, Université de Reims Champagne-Ardenne, pp.3

[2] DONA Victorien Bruno, 'Modelisation et conversion des irradiations solaires en vue de la production d'énergie rénouvelable à Mahajanga', Habilitation to direct research, University of Mahajanga, Madagascar, August 28, 2019.

[3] T. Mrabbti, K. Loudiyi, H. Darhmaoui, K. Kassmi, A. El Moussaoui, et al. Implantation et fonctionnement de la première installation photovoltaïque à haute concentration 'CPV' au Maroc, Revue des Energies Renouvelables Vol. 15 N°2 (2012) 351 -356.

[4] PASERA Joanès Keneddy, HARITHI BEN Daoud Ben Attoumane, DONA Victorien Bruno, 'Influence of Cooling Systems on a Dual-Fluid CPVT Solar Concentrator (Water and Air)', IJERD Vol. 21 N°6 (2025), PP 69-83. Available at SSRN: https://ssrn.com/abstract=5336414 or http://dx.doi.org/10.2139/ssrn.5336414

[5] TOUAFEK Khaled, 'Contribution à l'étude et à la conception d'un système énergétique utilisant des capteurs hybrides photovoltaïques thermiques', Thesis, Ecole Normale Polytechnique ENP, Algeria, 2010.

[6] Laarabi El Oussoul, Achour Elhamdaouy, Abdessalam Ait Madi, ' A new MPPT control strategy based on a weighting mechanism: Enhancing effiiency in solar energy harvesting', Results in Engineering 26 (2025) 104725, https://doi.org/10.1016/j.rineng.2025.104725

[7] Ambe Harrison, C. Feudjio, C. R. F. Mbobda, N. Henry Alombah, 'A new framework for improving MPPT algorithms through search space reduction', Results in Engineering 22 (2024) 101998, https://doi.org/10.1016/j.rineng.2024.101998

[8] PASERA Joanès Keneddy, HARITHI BEN et DONA Victorien Bruno, 'Performance Analysis of a Dual-Fluid CPVT Solar Concentrator (Water and Air)', IJERD e-ISSN: 2278-067X, p-ISSN:2278-800X, Vol 21, Issue 5 (May 2025), PP 116-129.

[9] Oussama El Manssouri, Chaimae E. F, Bekky H et al., 'Mass Flow Rates Effect on the Performance of PV/T Bifluid Hybride Collector (Single and Simultaneous Modes)'.,2021, in Electrical Engineering 681,

[10] S. Ben Mabrouk, 'Etude et Simulation d'un Capteur hybride Photovoltaique Thermique à air', University of Tunis El Manar, Researchgate, 2016.

[11] MEKADEM Hafsa et Mellouki H., 'Etude paramétrique d'un capteur hybride doté d'un concentateur parabolique composé (PVT- CPC)', Mémoire, Université Ahmed Draia-Adrar, 2022.

[12] TABET Ismail. 'Etude, Réalisation et simulation d'un capteur solaire', thèse, Université des freres mentouri constantine, 2016.

[13] PASERA Joanès Keneddy, HARITHI BEN et DONA Victorien Bruno, 'Thermal efficiency of the Photovoltaic-Thermal aircoupled Parabolic through-Heliostat Concentrator (PVT-CCPH)', IJARIIE-ISSN(O)-2395-4396, Vol-10 Issue-6 2024.

[14] Incropera, F.P.; DeWitt, D.P. 'Fundamentals of Heat and Mass Transfer', 6th ed.; John Wiley & Sons, Inc.: Hoboken, NJ, USA, 2007.

[15] GHELLAB Amel, 'Modélisation et optimisation des capteurs solaires hybrides', Thèse, Université des frères Mentours Constantine, 2018

[16] AKERMI Mustapha, 'Modelisation, simulation et analyse de comportement d'un capteur solaire plan à eau pour différents sites en ALGERIE'., These, Université Abou-bekr belkaid-Tlemcen, 2019.

[17] Bourouaiah Yassine, Kimouche Fouaz., 'Etude numérique des performances d'un capteur solaire plan à eau'., Memoire, Université Mohamed Seddik Ben Yahia – Jijel, 2021

[18] HADJIAT Mohammed Moundji, 'Modelisation et realisation d'un capteur-stockeur solaire à cuve cylindrique avec concentrateur parabolique compose', These, Université Abou-Bekr Belkaid-Tlemcen, 2014, pp.38

[19] BOUHOREIRA Y. and GANA L. 'Etude de l'effet des paramètres sur les performances d'un collecteur solaire cylindro parabolique', mémoire, Université Kasdi Merbah Ouargla, 24-06-2018.

[20] René RAUD, Chapidtre I DOSSIER DE CALCULS-soleil-vapeur,

[21] PASERA Joanès Keneddy, HARITHI BEN et DONA Victorien Bruno, « Optimizing the energy performance of a hybrid PVT air collector with Parabolic trough concentrator and Heliostat», IJARIIE-ISSN(O)-2395-4396, Vol-10 Issue-5 2024

[22] Oussama El Manssouri, B. Hajji, Giuseppe M.T, Antonio G. and Stefano A., 'Electrical and Thermal Performances of Bi-Fluid PV/Thermal Collectors'. Energies 2021, 14, 1633.

[23] M.Y. Othman, S.A. Hamid et al., Performance analysis of PV/T Combi with water and air heating system: An experimental study.Renewable Energy 86 (2016) 716e722

[24] Nurul Shahirah Rukman, Ahmad F. et al., Bi-fluid cooling effet on electrical characteristics of flexible photovoltaic panel., Journal of Mechatronics, Electrical Power, and Vehicular Technology 12 (2021) 51 -56

[25] Mohammad Sardarabadi, Mohammad P., Experimental and numerical study of metal-oxides/water nanofluids as coolant in photovoltaic thermal systems (PVT)., Solar Energy Materials & Solar Cells 157 (2016) 533–542

[26] Hasila Jarimi, Mohd Nazari A. B., et al., Bi-fluid photovoltaic/thermal (PV/T) solar collector: experimental validation of a 2-D theoretical model., Renewable Energy 85 (2016) 1052 e1067

[27] Juwel Chandra Mojumder, Wen Tong C., et al., An experimental investigation on performance analysis of air type photovoltaic thermal collector system integrated with cooling fins design.

[28] M. ABOUCHABANA Nabil, 'Etude d'une nouvelle topologie buck-boost appliquée à un MPPT', Mémoire, Université Amar Telidji de Laghouat, (2009)

[29] SAHRAOUI Hamza, 'Modélisation Et Commande Des Convertisseurs DC-DC Utilisés Dans Les Systèmes Photovoltaïques (Théorie et Expérimentation)', These, Université de Batna 2, (2016)

[30] NASRI Sabrine et BEN Hamida Ouissem, 'ETUDE ET SIMULATION D'UN HACHEUR (BUCK-BOOST)', Mémoire, Université BADJI MOKHTARAnnaba, (2021).

[31] Saima Siouana, Slavisa Jovanovic and Philippe Poure, 'Service Continuity of PV Synchronous Buck/Buck-Boost Converter with Energy Storage', *Energies* **2018**, *11*, 1369; doi:10.3390/en11061369

[32] BETTOUCHE Mohamed Amine, REDJRADJ Adel, 'Etude, dimensionnement et simulation d'un système hybride photovoltaïque-diesel alimentant une habitation isolée', Mémoire, Université de A-MIRA de BEJAIA (2016)

[33] Félix-Antoine LeBel, 'Méthode de dimensionnement et modélisation de batteries lithium-ion', Mémoire, Université de Sherbrooke, (2017).

[34] BELKACEM Mourad, 'Etude et optimisation du transfer d'énergie électrique en conversion photovoltaïque par la recherche du point de puissance maximal (MPPT)', Mémoire, Université Abou Belkaid de Tlemcen, 2015

[35] INERGY, SR-300-48 LiFePO4 Household Energy Storage Battery Pack Specification.pdf, https://inergy.mg/lithium/395-batterie-300ah-48v-lithium-titan-.html

[36] Victron Energy, Convertisseur/chargeur Quattro 277V 15kVa, https://www.solaris-store.com/1064-quattro-48-10000-140-100-100-230v-vebus-victron-qua481030010.html